

CrossMark
click for updatesCite this: *J. Mater. Chem. A*, 2015, 3, 6291Received 31st December 2014
Accepted 16th February 2015

DOI: 10.1039/c4ta07208a

www.rsc.org/MaterialsA

A new approach towards the synthesis of nitrogen-doped graphene/MnO₂ hybrids for ultralong cycle-life lithium ion batteries†

Tingzhou Yang, Tao Qian,* Mengfan Wang, Jie Liu, Jinqiu Zhou, Zhouzhou Sun, Muzi Chen and Chenglin Yan*

A new approach using polypyrrole as the nitrogen source has been demonstrated for the fabrication of nitrogen-doped graphene, which subsequently served as nucleation centers for the growth of metal oxides. The thin layers of the nitrogen-doped graphene are not only used as conductive pathways accelerating the electrical conductivity of metal oxides but also serve as buffer layers to improve the electrical contact with metal oxide nanostructures during the delithiation/lithiation of lithium ions. As anodes for lithium ion batteries, the nitrogen-doped graphene and their hybrids with MnO₂ nanorods exhibit exceptionally excellent capacity retention for 3000 cycles at 2500 mA g⁻¹, and ultrafast rate capability, which pave the way for developing electrode materials for long cycle-life energy storage devices.

Introduction

Nitrogen-doped graphene, a kind of graphene derivative, exhibits excellent reliability, high capacity and enhanced lithium storage properties. In addition, N-doped structures can adjust the band structure of graphene without reducing its conductivity.¹⁻³ Further studies reveal that nitrogen doping seems to be the most appropriate method for strengthening the surface wettability of materials, capacity, and electronic conductivity while maintaining superior cycle capability.⁴ Some methods have been proposed to prepare N-doped graphene, such as chemical vapor deposition (CVD),⁴ heating graphene with nitrogen rich compounds,⁵ annealing graphite oxide (GO) in NH₃ and so on.⁶ Among them, CVD is the most common method to synthesize N-doped graphene by using methane (CH₄) as the carbon source and NH₃ (ref. 7) or pyridine⁸ as the nitrogen source *via* depositing on a nickel or copper substrate at

a high temperature of 1000 °C. It's worth noting that doping of metal impurities into N-doped graphene can affect the real performance of materials. Moreover, the use of CH₄, H₂, NH₃ and pyridine at high temperature is poisonous and dangerous. To address the above issues, we report a novel method using polypyrrole (PPy) as the N source for the fabrication of high-quality N-doped graphene.

Graphene based materials have been widely used in many fields, such as energy, electronics, biology, and catalysis⁹⁻¹¹ due to their excellent electron transport properties, distinguished conductivity, large surface area, and chemical properties. Lithium ion batteries are integral power sources in several current technologies.¹² With the development of electronic products and electric vehicles, much progress has been made in achieving fast charging and discharging rates for lithium ion batteries.^{13,14} Various transition-metal oxides, such as Co₃O₄,¹⁵ NiO,¹⁶ MnO₂,^{17,18} MoO₂,¹⁹ TiO₂ (ref. 20) and V₂O₅,²¹ have been widely used in lithium-ion batteries. They are confirmed to have ultrahigh energy density values because of their unique conversion reactions.²² Among all of the transition metal oxides, manganese oxide (MnO₂), which is naturally abundant, cost-effective and environmentally friendly, has been known as the promising electrode material for lithium-ion batteries.²³⁻²⁵ However, the problems of large volume changes and particulate matter aggregation during the process of intercalation and de-intercalation of lithium ions result in poor cycling stability and low electrical conductivity (10⁻⁵ to 10⁻⁶ S cm⁻¹).²⁶⁻²⁹ To solve these problems, it is necessary to find electrode materials which could promote the electron and ion diffusion coefficient simultaneously. Until now, studies on different kinds of MnO₂ nanostructure/graphene composites have been reported. As reported by Li *et al.*, MnO₂ nanostructures grown on graphene sheets only afforded a low capacity of 230 mA h g⁻¹ at a current density of 200 mA g⁻¹ after 150 cycles.³⁰ Yu *et al.* showed that the graphene-MnO₂ nanotube material exhibits a low capacity of 100 mA h g⁻¹ at a current density of 495 mA g⁻¹.³¹ Sun *et al.* reported that MnO₂ hierarchical nanostructures deliver an increased capacity of 381 mA h g⁻¹ at a rate of 100 mA g⁻¹

College of Physics, Optoelectronics and Energy & Collaborative Innovation Center of Suzhou Nano Science and Technology, Soochow University, Suzhou 215006, China.
E-mail: c.yan@suda.edu.cn; tqian@suda.edu.cn

† Electronic supplementary information (ESI) available. See DOI: 10.1039/c4ta07208a

between 0.02 and 3.20 V.¹⁸ However, it is critically important for lithium ion batteries to have long cycle life, and high energy and power densities at rapid charge and discharge rates.

In the present work, a novel concept of synthesizing N-doped graphene has been demonstrated using polypyrrole (PPy) as the N source. Graphene oxide (GO) is firstly in cocoon by PPy *via in situ* polymerization (PPy/GO). During the carbonization process, N atoms in pyrrole rings may be easily converted to the graphene structure, and yields a higher content of nitrogen (about 5.04 at%) than the previous methods.^{32–34} Then MnO₂ nanorods decorated with N-doped graphene (MnO₂/NG) are fabricated facilely through a solution-based reaction. N-doped graphene enhances the ion and electron diffusion within the hybrid electrodes, resulting in high electronic conductivity. Furthermore, the excellent mechanical flexibility of N-doped graphene layers provides space for MnO₂ nanorods for volume accommodation during the repeatable cycling process, which eventually results in enhanced cyclability at an ultrafast charge-discharge rate.

Experimental section

Synthesis of the N-doped graphene

Graphene oxide (GO) was synthesized using modified Hummer's method.³⁴ The PPy/GO was prepared by the addition of 2.5 ml H₂O₂ to the GO/pyrrole/FeCl₂/H₂O (100 mg/0.5 ml/0.05 g/100 ml) mixture and allowed to stand for 6 hours. Then, the PPy/GO was annealed in a quartz tube under the protection of the N₂ atmosphere (150 sccm) at a heating rate of 10 °C min⁻¹ to a carbonization temperature (500 °C, 700 °C, 900 °C, and 1100 °C each for 2 h) to prepare N-doped graphene nanosheets.

Synthesis of the MnO₂/NG composite

The MnO₂/NG composite was prepared by the hydrothermal synthesis method. The reaction solution was obtained by mixing 11 mg KMnO₄ and 8 mg N-doped graphene nanosheets in 10 ml of deionized water under adequate stirring and then transferred into a Teflon-lined stainless steel autoclave. The autoclave was maintained at 220 °C for 24 h, and then cooled down to room temperature.

General characterization

Field emission scanning electron microscopy (FESEM) imaging and field emission transmission electron microscopy (FETEM) were performed on a SU8010, Hitachi, Ltd and a FEI Tecnai G220, FEI NanoPorts, Ltd. Surface elemental analysis was performed on an X-ray photoelectron spectrometer (XPS, Kratos Axis Ultra Dld, Japan) and a Powder X-ray Diffractometer (XRD, X'Pert-Pro MRD, Philips). Thermogravimetric analysis (TGA, SDT 2960, USA) was performed on an SDT 2960, TA Instruments. The elemental analysis was performed using a Vario MICRO CUBE (Elementar Analysensysteme GmbH).

Electrochemical characterization

The working electrodes were prepared by thoroughly mixing 70 wt% active materials, 20 wt% acetylene black, and 10 wt%

polytetrafluoroethylene (PTFE, 60 wt% dispersion in water) on a titanium foil (0.1 mm). After drying in a vacuum at 60 °C for 6 h, the battery was made in a glove box (Shanghai Mikrouna Mech. Tech. Co., Ltd), where the electrolyte was LiPF₆ (1 M) in ethylene carbonate (EC) and dimethyl carbonate (DMC) (1 : 1, v/v). The galvanostatic charge-discharge test and cyclic voltammetry were performed in the voltage range of 0.0–3.0 V on a CT2001A cell test instrument (Wuhan LAND Electronic Co., Ltd) and a CHI 660E (Shanghai Chenhua instrument Co., Ltd) electrochemical workstation, respectively.

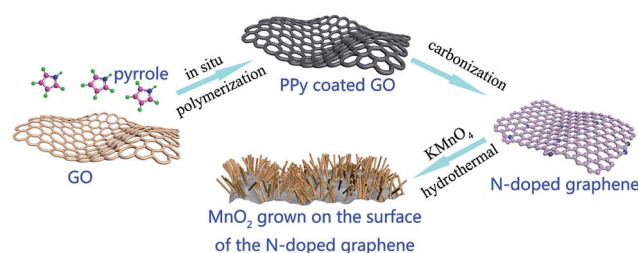
Results and discussion

Our controlled synthesis of the MnO₂/NG hybrids is illustrated in Scheme 1. GO sheets are coated with PPy layers by π - π and electrostatic interactions through *in situ* polymerization. As the neighbor of C in the periodic table, the N atoms in pyrrole rings convert to the graphene structure *via* the decomposition of PPy in the carbonization process.^{6,35} The prepared N-doped graphene then served as nucleation centers for the deposition of MnO₂ nanorods, which can be described as follows:^{30,36}



The general structure, size and morphology of the MnO₂/NG composite were investigated by scanning electron microscopy (SEM) and transmission electron microscopy (TEM) (Fig. 1). It is obvious that the dense PPy/GO nanostructures (Fig. S1A†) become thin and transparent nanosheets with 3D structures (N-doped graphene, Fig. S1B†) after carbonization. The sufficient distance between nanosheets is loose and suitable for the growth of MnO₂ nanorods. It can be seen (Fig. 1A and B) that each of the MnO₂ nanostructures is nanorod-shaped, which is several micrometers in length and grows on the surface of N-doped graphene uniformly. Fig. 1C shows a TEM image of deposited MnO₂ nanorods with an average diameter of about 108 nm. For more details, the crystalline nature of MnO₂ nanorods is presented in Fig. 1D, which reveals a crystal lattice space of 0.35 nm for the crystalline MnO₂ nanostructures.

The X-ray diffraction (XRD) pattern of MnO₂/NG samples is displayed in Fig. 2A. Broad and strong peaks around 44.5° and 26° are observed, arising from the (002) and (100) crystal planes of N-doped graphene. The peaks located at 65.5°, 44.3°, 42.6°, 38.8°, 34.4°, 32.8°, and 28.8° belong to the (002), (521), (131),



Scheme 1 Schematic representation of the preparation of the PPy/GO, N-doped graphene, and MnO₂/NG hybrids.

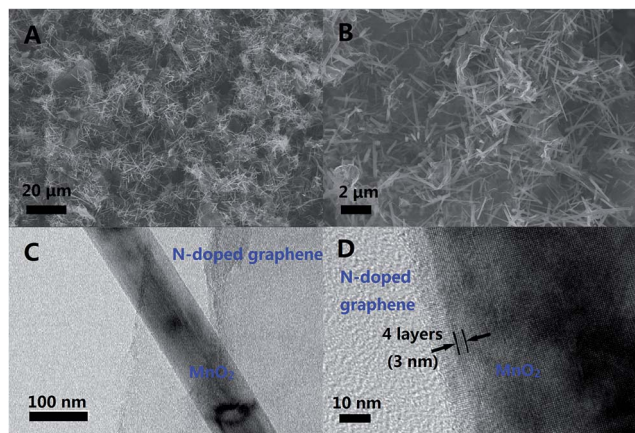


Fig. 1 (A) Low-magnification and (B) high-magnification SEM images of MnO₂ nanorods grown on the N-doped graphene sheets; (C) TEM image of MnO₂/NG; (D) high resolution TEM of MnO₂/NG with partial enlarged view.

(031), and (310) planes of MnO₂. All the diffraction peaks of the assembled MnO₂/NG correspond to individual N-doped graphene and MnO₂ nanostructure indices. X-ray photoelectron spectroscopy (XPS) analysis was performed to identify the chemical components of the as-prepared product. From careful inspection of wide region spectroscopy and elemental analysis, the characteristic signals attributed to C, N, O, and Mn can be observed distinctly (Fig. 2B), which reveal the existence of N and Mn components. Fig. S2† shows the high-resolution XPS spectra for C, N, O and Mn. The core level peak of C1s can be resolved

into three components centered at 284.7 eV, 285.3 eV, and 286.3 eV (ref. 37) (Fig. S2A†) representing sp²C–sp²C, N–sp²C and N–sp³C bonds, respectively. In addition, it could be observed that the spectrum of N1s is resolved into three components centered at 389.9 eV, 401.2 eV (Fig. S2B†), and 402.7 eV,³⁷ corresponding to pyridinic N, pyrrolic N, and graphitic N (Fig. 2C), which indicate the existence of N-doped graphene. The peaks centered at 642.2 eV and 653.8 eV represent Mn2p_{3/2} and Mn2p_{1/2} (Fig. S2C†),¹⁷ and the peaks at 530.4 eV and 531.7 eV represent O–Mn and O–C (Fig. S2D†),²⁵ confirming the synergistic presence of MnO₂ in the composite. Moreover, thermogravimetric analysis (TGA) (Fig. 2D) demonstrates that the weight loss of the MnO₂/NG composites is around 68.78% at 800 °C, revealing that the content of MnO₂ in the MnO₂/NG is 31.22%.

To express the unique superiority of electrochemical properties of the MnO₂/NG, electrodes were directly investigated using half cells *versus* Li/Li⁺. Cyclic voltammetry (CV) was used to analyze the charge storage behaviors at a slow scan rate of 0.6 mV s⁻¹ between 0.01 V and 3 V. From the first cycle of Fig. 3A, it is clear that the curve in the first process is different from the subsequent ones. The peak at 0.35 V in the first cycle is assigned to the formation of a solid electrolyte interface (SEI) on the electrode surface and the reduced reaction of the MnO₂ and Li ions. The electrochemical oxidation reaction of solid electrolyte interface layers can be proved by two oxidation peaks at 1.3 V and 2.3 V. After the first cycle, it is obviously observed that the peaks of the follow-up curves are nearly unchanged, which demonstrates excellent structural stability and electrochemical reversibility of the MnO₂/NG. The electrochemical performance had been further examined by representative discharge–charge

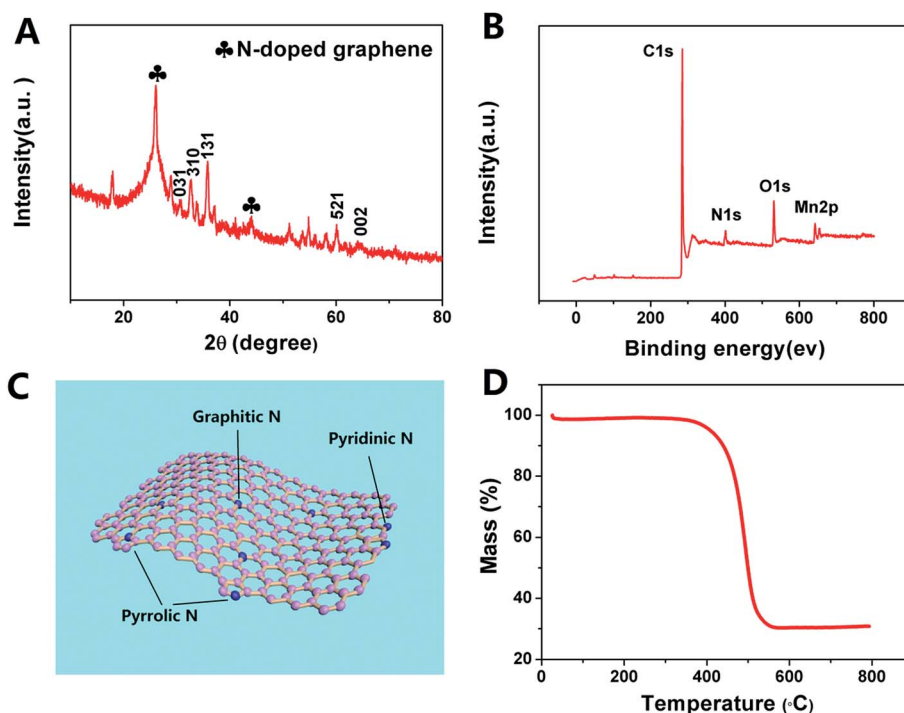


Fig. 2 (A) XRD pattern and (B) XPS spectrum of MnO₂/NG. (C) The explanatory diagram of the different N functionalities in the N-doped graphene. (D) The TGA between 0 °C and 800 °C at an increasing rate of 10 °C min⁻¹.

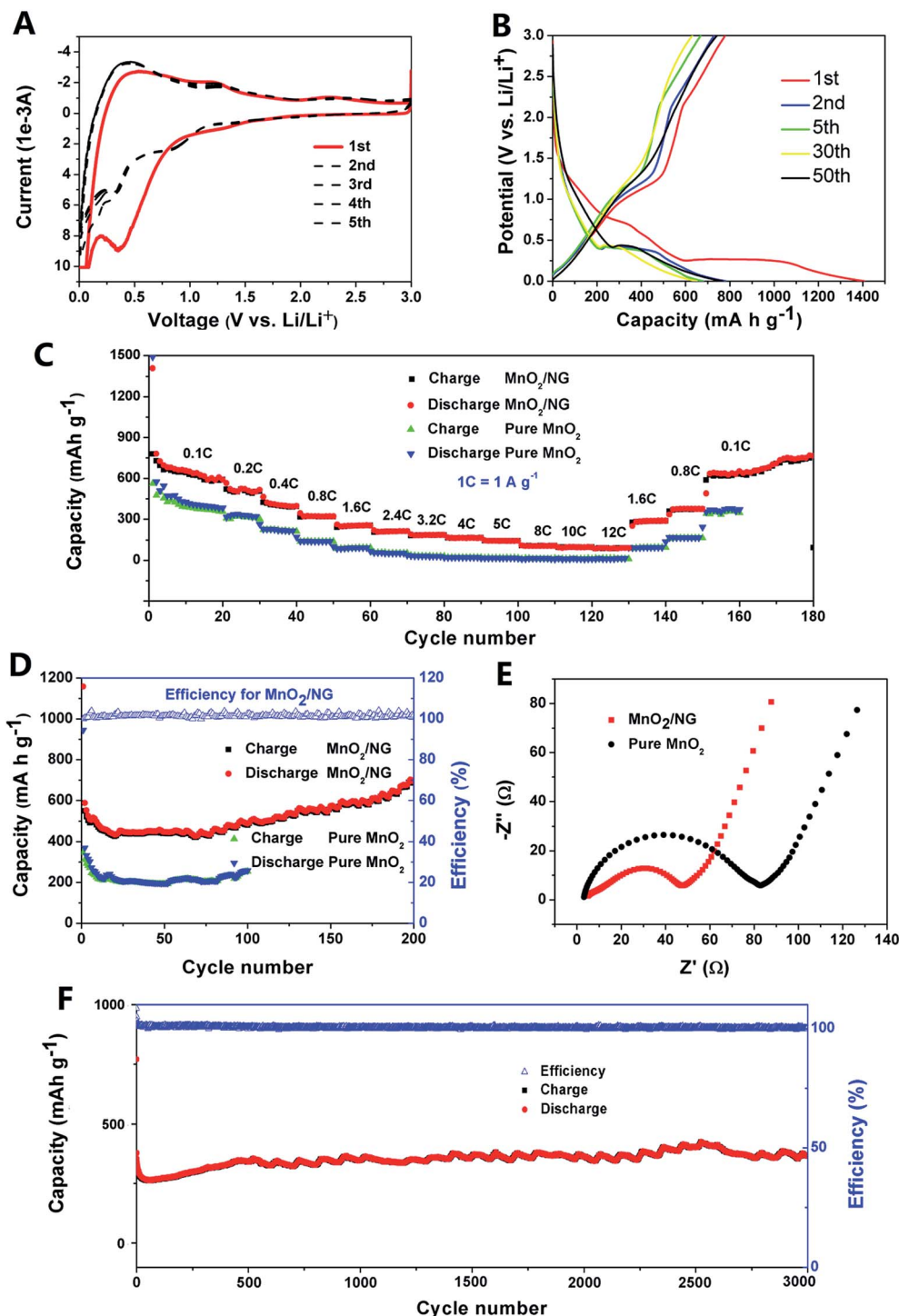


Fig. 3 (A) The foundation test of the electrochemical properties by the cyclic voltammetry obtained in a voltage range of 0.01 to 3 V (vs. Li^+/Li) and a potential scan rate of 0.6 mV s^{-1} . (B) Galvanostatic charge/discharge profile for the first, second, fifth, tenth, and fiftieth cycles of the MnO_2/NG anode at a current density of 100 mA g^{-1} . (C) Rate performance of the MnO_2/NG composite and pure MnO_2 . (D) Cycling performance of the MnO_2/NG anode and pure MnO_2 at a current density of 300 mA g^{-1} , and the efficiency is plotted on the right axis. (E) Nyquist plots of the MnO_2/NG and bare MnO_2 anode in the fresh coin cells over the frequency range of 0.1 Hz to 100 kHz. (F) Long-term cycling performance of the MnO_2/NG anode at a high current density of 2500 mA g^{-1} , and the efficiency is plotted on the right axis (blue circles).

voltage profiles at 1 C ($1 \text{ C} = 1000 \text{ mA g}^{-1}$) between 0 and 3 V (Fig. 3B). The initial discharge and charge capacities are found to be $1410.6 \text{ mA h g}^{-1}$ and $780.0 \text{ mA h g}^{-1}$. The capacity loss

may be caused by SEI formation as well as decomposition of the electrolyte during the first electrochemical reaction. This characteristic is also consistent with the peaks appearing in the first

scan while disappearing afterward in CV curves. The discharge voltage plateau at 0.28 V in the first discharge process is different from the plateau of other cycles at 0.41 V, which points out that irreversible reactions occurred in the first cycle process. During the next cycles of the charge and discharge process, the plateaus at 0.41 V are nearly unchanged, further indicating that the electrode of the MnO₂/NG mixture has excellent stable performance.

The cycling performance of MnO₂/NG was evaluated in the potential window of 0 to 3 V (Fig. 3C). At a current density of 100 mA g⁻¹, the discharge capacity tends to stabilize at about 647.5 mA h g⁻¹ after five cycles and rise slowly. Moreover, the MnO₂/NG battery was evaluated by the galvanostatic discharge/charge test at various current rates. From Fig. 3C, it can be seen that the discharge capacity varies as 607.5 mA h g⁻¹, 511.7 mA h g⁻¹, 415.5 mA h g⁻¹, 320.7 mA h g⁻¹, 253.4 mA h g⁻¹, 212.0 mA h g⁻¹, 184.9 mA h g⁻¹, 163.3 mA h g⁻¹, 143.1 mA h g⁻¹, 104.4 mA h g⁻¹, 94.4 mA h g⁻¹, and 90.0 mA h g⁻¹ with increasing current rates of 0.1 C, 0.2 C, 0.4 C, 0.8 C, 1.6 C, 2.4 C, 3.2 C, 4 C, 5 C, 8 C, 10 C, and 12 C. The capacity then increases back to 286.7 mA h g⁻¹, 375.6 mA h g⁻¹, and 638.6 mA h g⁻¹ when the current rate returns to 1.6 C, 0.8 C, and 0.1 C. By returning to the initial rate of 100 mA g⁻¹, the discharge capacity could almost return back to the original capacity, which can further demonstrate the elite performance of the fast and efficient transport of ions/electrons. By contrast, the pure MnO₂ electrode exhibits low discharge capacities, which illustrate that the improved rate performance is most likely due to the superior electronic conductivity of the N-doped graphene.

To ensure a fair comparison of the excellent stability, the electrochemical performance was investigated at a current rate of 300 mA g⁻¹ (Fig. 3D). The reconstituted N functional groups of N-doped graphene sheets are vital for improving their redeposition process upon discharge/charge. Also, the discharge/charge process shows perfect cycling stability and relatively high specific capacity during the 200th cycle. In addition, the coulombic efficiency of the anode retains nearly 100% after the second cycle, further indicating its excellent reversibility. The electrochemical impedance spectroscopy (EIS) measurements are shown in Fig. 3E, which can further explain the superior electrochemical performance. Due to excellent electrical conductivity and the surface capacitive effects of N-doped graphene, charge transfer and inherent resistances of the MnO₂/NG's are lower than those of bare MnO₂ electrodes, indicating superior conductivity which is beneficial for the rate capability enhancement. Furthermore, the MnO₂/NG composites are then tested at a high current density of 2500 mA g⁻¹ (Fig. 3F), where the capacity retention can reach almost 100% after 3000 cycles, further confirming the extremely long cycle-life of lithium ion batteries.

Conclusions

In summary, we present a novel and facile approach for fabricating high quality N-doped graphene, which can easily control the surface attractive force of the local electronic structures and enhance binding with Li-ions. The sufficient distance between

each N-doped graphene sheets is suitable for volume accommodation of the MnO₂ electrode during the ultrafast charge-discharge process. The as-prepared N-doped graphene/MnO₂ electrode battery exhibits ultralong cycle life exceeding 3000 cycles (at a current density of 2500 mA g⁻¹) and a remarkable reversible capacity of 638.6 mA h g⁻¹ at a current density of 100 mA g⁻¹, which provides great application potential to meet the high performance requirements of power sources.

Acknowledgements

We acknowledge the support from the "Thousand Talents Program", the Natural Science Foundation of Jiangsu Province of China (no. BK20140315), the National Natural Science Foundation of China (no. 51402202), the National Basic Research Program of China (no. 2015CB358600), the Jiangsu Shuangchuang Plan, and the Priority Academic Program Development of Jiangsu Higher Education Institutions (PAPD).

Notes and references

- 1 Y. Y. Shao, S. Zhang, M. H. Engelhard, G. S. Li, G. C. Shao, Y. Wang, J. Liu, A. I. Aksay and Y. H. Lin, *J. Mater. Chem.*, 2010, **20**, 7491.
- 2 Y. Z. Xue, B. Wu, Q. L. Bao and Y. Q. Liu, *Small*, 2014, **10**, 2975.
- 3 Y. Ito, H. J. Qiu, T. Fujita, Y. Tanabe, K. Tanigaki and M. W. Chen, *Adv. Mater.*, 2014, **26**, 4145.
- 4 L. F. Chen, X. D. Zhang, H. W. Liang, M. G. Kong, Q. F. Guan and P. Chen, *ACS Nano*, 2012, **6**, 7092.
- 5 S. Gilje, S. Han, M. S. Wang, K. L. Wang and R. B. Kaner, *Nano Lett.*, 2007, **7**, 3394.
- 6 Z. Q. Luo, S. H. Lim, Z. Q. Tian, J. Z. Shang, L. F. Lai, B. MacDonald, C. Fu, Z. X. Shen, T. Yu and J. Y. Lin, *J. Mater. Chem.*, 2011, **21**, 8038.
- 7 N. Li, Z. Y. Wang, K. K. Zhao, Z. J. Shi, Z. N. Gu and S. K. Xu, *Carbon*, 2010, **48**, 255.
- 8 L. S. Panchakarla, K. S. Subrahmanyam, S. K. Saha, A. Govindaraj, H. R. Krishnamurthy, U. V. Waghmare and C. N. R. Rao, *Adv. Mater.*, 2009, **21**, 4726.
- 9 T. Qian, C. F. Yu, S. S. Wu and J. Shen, *J. Mater. Chem. A*, 2013, **1**, 6539.
- 10 F. Withers, T. H. Bointon, M. F. Craciun and S. Russo, *ACS Nano*, 2013, **7**, 5052.
- 11 S. Borini, R. White, D. Wei, M. Astley, S. Haque, E. Spigone, N. Harris, J. Kivioja and T. Ryhanen, *ACS Nano*, 2013, **7**, 11166.
- 12 B. Kang and G. Ceder, *Nature*, 2009, **458**, 190.
- 13 H. G. Zhang, X. D. Yu and P. V. Braun, *Nat. Nanotechnol.*, 2011, **6**, 277.
- 14 Y. C. Qiu, W. F. Li, W. Zhao, G. Z. Li, Y. Hou, M. N. Liu, L. S. Zhou, F. M. Ye, H. F. Li, Z. H. Wei, S. H. Yang, W. H. Duan, Y. F. Ye, J. H. Guo and Y. G. Zhang, *Nano Lett.*, 2014, **14**, 4821.
- 15 W. Y. Li, L. N. Xu and J. Chen, *Adv. Funct. Mater.*, 2005, **15**, 851.

- 16 S. A. Needham, G. X. Wang and H. K. Liu, *J. Power Sources*, 2006, **159**, 254.
- 17 L. Li, A. O. Raji and J. M. Tour, *Adv. Mater.*, 2013, **25**, 6298.
- 18 D. F. Sun, J. T. Chen, J. Yang and X. B. Yan, *CrystEngComm*, 2014, **16**, 10476.
- 19 C. B. Zhu, X. K. Mu, P. A. Aken, J. Maier and Y. Yu, *Adv. Energy Mater.*, 2014, 1401170.
- 20 W. X. Guo, X. Y. Xue, S. H. Wang, C. J. Lin and Z. L. Wang, *Nano Lett.*, 2012, **12**, 2520.
- 21 T. Qian, N. Xu, J. Q. Zhou, T. Z. Yang, X. J. Liu, X. W. Shen, J. Q. Liang and C. L. Yan, *J. Mater. Chem. A*, 2015, **3**, 488.
- 22 P. P. S. Laruelle, S. Grugeon, L. Dupont and J. M. Tarascon, *Nature*, 2000, **407**, 496.
- 23 J. Cabana, L. Monconduit, D. Larcher and M. R. Palacín, *Adv. Mater.*, 2010, **22**, E170.
- 24 L. F. Chen, Z. H. Huang, H. W. Liang, Q. F. Guan and S. H. Yu, *Adv. Mater.*, 2013, **25**, 4746.
- 25 Z. S. Wu, W. C. Ren, D. W. Wang, F. Li, B. L. Liu and H. M. Cheng, *ACS Nano*, 2010, **4**, 5835.
- 26 X. Y. Lang, A. Hirata, T. Fujita and M. W. Chen, *Nat. Nanotechnol.*, 2011, **6**, 232.
- 27 X. Y. Han, F. Zhang, Q. F. Meng and J. T. Sun, *J. Am. Ceram. Soc.*, 2010, **93**, 1183.
- 28 L. Y. Yuan, X. H. Lu, X. Xiao, T. Zhai, J. J. Dai, F. C. Zhang, B. Hu, X. Wang, L. Gong, J. Chen, C. G. Hu, Y. X. Tong, J. Zhou and Z. L. Wang, *ACS Nano*, 2012, **6**, 656.
- 29 H. Lai, J. X. Li, Z. G. Chen and Z. G. Huang, *ACS Appl. Mater. Interfaces*, 2012, **4**, 2325.
- 30 J. X. Li, Y. Zhao, N. Wang, Y. H. Ding and L. H. Guan, *J. Mater. Chem.*, 2012, **22**, 13002.
- 31 A. P. Yu, H. W. Park, A. Davies, D. C. Higgins, Z. G. Chen and X. C. Xiao, *J. Phys. Chem. Lett.*, 2011, **2**, 1855.
- 32 F. H. Du, B. Li, W. Fu, Y. J. Xiong, K. X. Wang and J. S. Chen, *Adv. Mater.*, 2014, **26**, 6145.
- 33 T. Qian, C. F. Yu, S. S. Wu and J. Shen, *Biosens. Bioelectron.*, 2013, **50**, 157.
- 34 W. S. Hummers Jr and R. E. Offeman, *J. Am. Chem. Soc.*, 1958, **80**, 1339.
- 35 X. R. Wang, X. L. Li, L. Zhang, Y. K. Yoon, P. K. Weber, H. I. Wang, J. Guo and H. J. Dai, *Science*, 2009, **324**, 768.
- 36 J. X. Li, N. Wang, Y. Zhao, Y. H. Ding and L. H. Guan, *Electrochem. Commun.*, 2011, **13**, 698.
- 37 A. L. M. Reddy, A. Srivastava, S. R. Gowda, H. Gullapalli, M. Dubey and P. M. Ajayan, *ACS Nano*, 2010, **4**, 6337.